# A Gray-Box Impedance Reshaping Method of Grid-Connected Inverter for Resonance Damping

Hu, Weihao; Wang, Yanbo; Cai, Pei; Chen, Zhe

*Published in:*
Proceedings of 2019 10th International Conference on Power Electronics and ECCE Asia (ICPE 2019 - ECCE Asia)



*Publication date:*
2019

*Document Version*
Accepted author manuscript, peer reviewed version

# A Gray-Box Impedance Reshaping Method of Grid-Connected Inverter for Resonance Damping

Weihua Zhou*, Yanbo Wang*, Pei Cai† and Zhe Chen*
*Department of Energy Technology, Aalborg University, Aalborg, Denmark
wez@et.aau.dk, ywa@et.aau.dk, zch@et.aau.dk
†School of Automation, Northwestern Polytechnical University, Xi'an, Shaanxi, China
pca@et.aau.dk

***Abstract*—Oscillation phenomenon of grid-connected inverter can be caused due to time-varying grid impedance. Terminal output impedance of inverter can be reshaped by re-tuning internal parameters of inverter to mitigate the oscillation issue. However, it's not easy to obtain internal parameters of grid-connected inverter in practical operation. This paper presents a gray-box parameters identification method to identify the parameters of LCL filter, the proportional coefficient of current controller and capacitor-current-feedback coefficient from the measured terminal impedance frequency responses by using vector fitting algorithm. When instability phenomenon of multiple-paralleled inverters system occurs, the internal parameters of each inverter are first identified by using the proposed method. Then, the capacitor-current-feedback coefficients are re-tuned to stabilize the studied power system according to the impedance-based stability criterion. The re-designed parameters for the specific grid condition can be delivered to the manufacturers for further parameters modification. Simulation results are given to validate the proposed gray-box parameter identification and corresponding impedance reshaping method.**

***Index Terms*—Capacitor-current-feedback coefficient, gray-box parameter identification, grid-connected inverter, impedance reshaping.**

## I. Introduction

Offshore wind power has been increasingly exploited due to abundant wind sources and constant wind speed [1]. Voltage source converter (VSC) with LCL filter is widely adopted as an important interface to deliver electricity to utility grid [2]. However, high-frequency oscillation phenomena can be triggered because of interaction between inner control loop and time-varying grid impedance [3]–[7]. Therefore, stability assessment methods and damping control strategies have been developed to deal with the oscillation phenomena.

The damping methods for single VSC have been widely presented in previous work, including passive damping [8], filter-based active damping [9], [10], and multi-loop-based active damping methods [11]–[13]. The passive damping methods tend to cause extra power loss and decrease system efficiency due to damping resistor [8]. Also, filter-based damping methods such as notch filter should align resonant frequency of LCL filter exactly with the center frequency of the notch filter, which is not effective once the parameters of LCL filter are perturbated [9], [10]. The multi-loop-based active damping methods are able to enhance stability by introducing additional control loop such as capacitor-current-feedback active damping loop, which have been paid much attentions [11]–[13]. Therefore, VSC with capacitor-current-feedback active damping is studied in this paper.

The effect of capacitor-current-feedback active damping on output impedance of VSC is investigated in [13]. However, re-tuning strategy of controller parameters is not further concerned to address stability under complicated grid conditions. In [14]–[16], controller parameters of active damping loop are tuned based on passivity-based analysis method to enhance system stability considering long transmission cable. And the design guidelines of controller parameters for these active damping methods are given. However, the accurate parameters of LCL filter and controller are important, which is difficult to be obtained from power plant operator due to industrial confidence.

Estimation and identification methods of controller and filter parameters have been proposed in [17]–[22]. In [17]–[19], the equivalent inductance and resistance of VSC are estimated to support optimization design of controller parameters, so that a desirable dynamic and steady performance can be achieved. However, no specific filter or controller parameters are estimated. The parameters of LCL filter are identified in [20]. In addition, the parameters of current controller and phase-locked loop (PLL) are identified with the assumption that the parameters of LCL filter are known in [21]. However, both [20] and [21] cannot simultaneously identify parameters of LCL filter and current controller. A two-step parameter identification method is proposed in [22], where the parameters of voltage/current controllers and filter inductance are identified. However, the identification method is not effective for LCL-filtered VSC.

This paper presents a gray-box impedance reshaping method for VSC, where the parameters of LCL filter, current control loop and capacitor-current-feedback loop are first identified from the measured terminal impedance frequency responses by vector fitting (VF) algorithm. If instability phenomenon occurs when the VSC is connected with weak grid, parameters of current control loop and active damping loop are re-tuned

This work was supported by the ForskEL and EUDP Project "Voltage Control and Protection for a Grid towards 100% Power Electronics and Cable Network (COPE)" (Project No.: 880063).

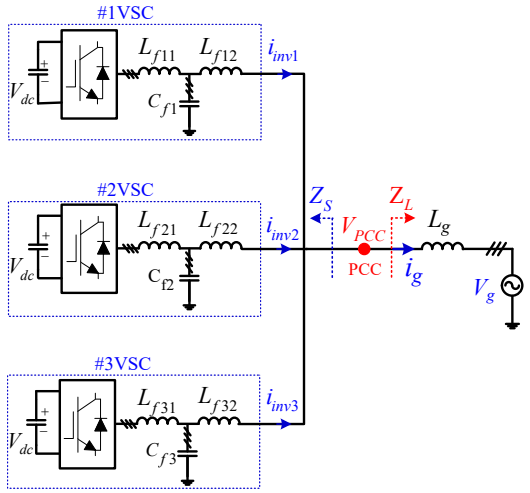


Fig. 1. Configuration of the studied power system.

to reshape the output impedance of the VSC, so that the undesired impedance interaction between the VSC and weak grid can be avoided, and the system can be brought to be stable.

## II. System Description and Impedance Modelling

In this section, the configuration of the studied power system is first described. Then, impedance model of VSC with capacitor-current-feedback active damping is established.

### A. Configuration of the Studied Power System

Fig. 1 shows configuration of the studied power system with three paralleled VSCs. The control diagram of current control loop for each VSC is shown in Fig. 2, where LCL filter is used to attenuate high-frequency current ripples. PLL is used to synchronize inverter with utility grid. $K_{vk}$ is the capacitor-current-feedback coefficient. $G_{cdqk}$ is the transfer function of current controller in dq reference frame. $G_{dk}$ represents time delay (1.5 $T_{sk}$) including computation delay and PWM delay.

Stability of the studied power system as shown in Fig. 1 can be assessed by identifying the impedance ratio $Z_L/Z_s = Z_L/(Z'_{inv1}//Z'_{inv2}//Z'_{inv3})$, where $Z'_{inv1}$, $Z'_{inv2}$ and $Z'_{inv3}$ are output impedance of #1VSC, #2VSC and #3VSC, respectively. When instability phenomenon occurs, output impedance of each VSC can be reshaped by retuning $K_{vk}$ and $K_{pk}$ to stabilize the system.

### B. Impedance Model of VSC with Capacitor-Current-Feedback Active Damping

Fig. 3 shows control diagram of grid-connected inverter with capacitor-current-feedback active damping. Output impedance of the VSC without consideration of capacitor-current-feedback active damping is first derived by neglecting the red dashed feedback line, shown as (1) [23].

$$Z_{invk} = \frac{L_{fk1}L_{fk2}C_{fk}s^3 + (L_{fk1}+L_{fk2})s + K_{pk}e^{-1.5sT_{sk}}}{L_{fk1}C_{fk}s^2 + 1} \tag{1}$$

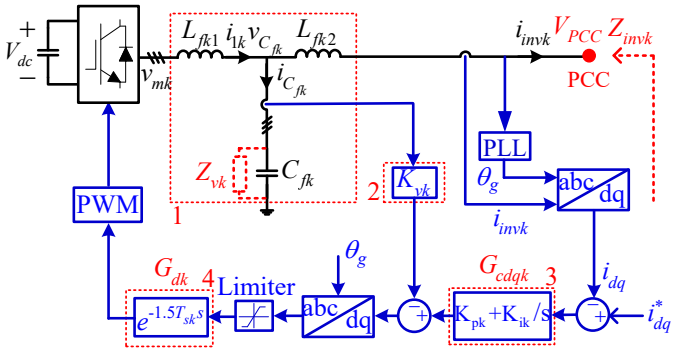


Fig. 2. Control diagram of grid-connected inverter #$k$VSC ($k = 1, 2, 3$) with capacitor-current- feedback active damping.

The active damping loop can be equivalent to a virtual impedance $Z_{vk}$ paralleled to $C_{fk}$ [24]. The equivalent virtual impedance can be derived as (2).

$$Z_{vk} = \frac{L_{fk1}}{K_{vk}C_{fk}G_{dk}} = \frac{R_{vk}}{G_{dk}} \tag{2}$$

Therefore, output impedance of the #$k$VSC with consideration of capacitor-current-feedback active damping can be obtained by modifying the output impedance formula in (2), shown as (3) on the next page.

A pure resistor $R_{vk}$ is defined as (4).

$$R_{vk} = \frac{L_{fk1}}{K_{vk}C_{fk}} = Z_{vk}G_{dk} \tag{4}$$

(3) can be represented as (5) based on (4).

$$Z_{invk'} = L_{fk2}s + \frac{L_{fk1}s + K_{pk}e^{-1.5sT_{sk}}}{L_{fk1}C_{fk}s^2 + \frac{L_{fk1}s}{R_{vk}}e^{-1.5sT_{sk}} + 1} \tag{5}$$

## III. The Proposed Gray-Box Impedance Reshaping Method

In this section, the gray-box parameter identification and controller re-tuning method is first developed, and the implementation procedure is then given.

### A. The Proposed Parameters Identification Method

The parameters of the LCL filter $L_{fk1}$, $L_{fk2}$ and $C_{fk}$, the proportional coefficient of the current controller $K_{pk}$ and the sampling period $T_{sk}$ have been identified from the measured terminal impedance frequency responses using VF algorithm in [25]. To implement the identification method considering capacitor-current-feedback loop, the parameter identification approach should be further developed.

Terminal impedance frequency responses can be fitted in s domain using vector fitting (VF) algorithm [26], as shown in (6).

$$f(s) = \frac{\sum_{i=0}^{M} B_i s^i}{\sum_{i=0}^{M} A_i s^i} + Zs \tag{6}$$

$$Z_{invk'} = \frac{L_{fk1}L_{fk2}C_{fk}s^3 + \frac{L_{fk1}L_{fk2}s^2}{Z_{vk}} + (L_{fk1}+L_{fk2})s + K_{pk}e^{-1.5sT_{sk}}}{L_{fk1}C_{fk}s^2 + \frac{L_{fk1}s}{Z_{vk}} + 1} \tag{3}$$

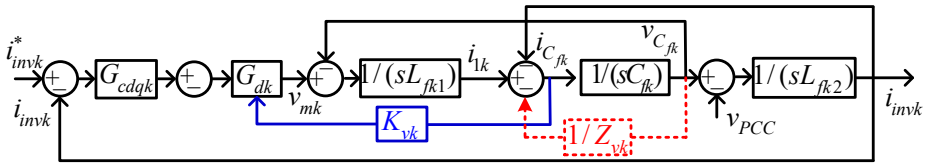


Fig. 3. The control block diagram of grid current control loop with capacitor-current-feedback active damping for the #$k$VSC ($k = 1, 2, 3$).

where the numerator and denominator are both in the form of $M$-order polynomial transfer function, and $Z$ is non-zero only if the order of the numerator is higher than the order of the denominator.

To identify the parameters of circuit and controller, the two exponential expressions in (5) should be represented by Pade approximation using appropriate orders, so that (5) can be in the same form of (6), and the parameters can be identified by comparing these coefficients. Therefore, the determination of order number of Pade approximations is a critical issue. $e^{-1.5sT_{sk}}$ in the nominator of (5) can be modelled in the form of (7) with the order of numerator $n$ and order of denominator $m$ [27].

$$e^{-1.5T_s s}_{num} = \frac{b_0 + ... + b_i s^i + ... + b_n s^n}{a_0 + ... + a_j s^j + ... + a_m s^m} \tag{7}$$

where $a_j = \frac{(n+m-j)!m!}{j!(m-j)!}(1.5T_s)^j$, $j = 0, 1..., m$, $b_i = (-1)^i \frac{(n+m-i)!n!}{i!(n-i)!}(1.5T_s)^i$, $i = 0, 1..., n$.

Similarly, the $e^{-1.5sT_{sk}}$ in the denominator of (5) can be represented by the Pade approximation with the order of numerator $q$ and order of denominator $p$, shown as (8).

$$e^{-1.5T_s s}_{den} = \frac{d_0 + ... + d_i(1.5T_s s)^i + ... + d_q(1.5T_s s)^q}{c_0 + ... + c_j(1.5T_s s)^j + ... + c_p(1.5T_s s)^p} \tag{8}$$

where $c_j = \frac{(q+p-j)!p!}{j!(p-j)!}(1.5T_s)^j$, $j = 0, 1..., p$, $d_i = (-1)^i \frac{(q+p-i)!q!}{i!(q-i)!}(1.5T_s)^i$, $i = 0, 1..., q$.

(5) can be transferred to be in the form of polynomial expression by substituting (7) and (8), shown as follows,

$$Z_{invk'} = L_{fk2}s + \frac{... + F_1 s + F_0}{... + E_1 s + E_0} \tag{9}$$

where only the several low-order components are shown in (9) for simplification. The detailed formulas are shown as (10).

$$\begin{aligned} F_1 &= L_{fk1}R_{vk}a_0c_0 + K_{pk}R_{vk}b_0c_1 + K_{pk}R_{vk}b_1c_0 \\ F_0 &= K_{pk}R_{vk}b_0c_0 \\ E_1 &= L_{fk1}a_0d_0 + R_{vk}a_0c_1 + R_{vk}a_1c_0 \\ E_0 &= R_{vk}a_0c_0 \end{aligned} \tag{10}$$

It can be found from (5), (6) and (10) that,

$$\begin{aligned} &L_{fk2} = Z \\ &\frac{F_0}{E_0} = K_{pk} = \frac{B_0}{A_0} \\ &\frac{F_1}{E_0} = L_{fk1} + K_{pk}(\frac{c_1}{c_0} + \frac{b_1}{a_0}) = \frac{B_1}{A_0} \\ &\frac{E_1}{E_0} = \frac{L_{fk1}}{R_{vk}} + \frac{c_1}{c_0} + \frac{a_1}{a_0} = \frac{A_1}{A_0} \end{aligned} \tag{11}$$

By substituting $b_1/a_0 = -na_1/ma_0$ into (11), $a_1/a_0$ can be expressed as (12).

$$\frac{a_1}{a_0} = (\frac{E_1}{E_0} - \frac{L_{fk1}}{R_{vk}} - (\frac{F_1}{E_0} - L_{fk1})/K_{pk})/(1 + \frac{n}{m}) \tag{12}$$

On the other hand, according to the Pade approximation, (13) can be obtained.

$$\frac{a_1}{a_0} = \frac{1.5m}{m+n}T_s \tag{13}$$

The following equation can be obtained by combining (12) and (13),

$$\frac{L_{fk1}}{K_{pk}} - \frac{L_{fk1}}{R_{vk}} - 1.5T_{sk} = \frac{F_1}{K_{pk}E_0} - \frac{E_1}{E_0} = \frac{B_1}{K_{pk}A_0} - \frac{A_1}{A_0} \tag{14}$$

In addition, by substituting $s = j\omega$ into (5), the terminal impedance can be expressed in frequency domain, as shown in (15). If both the numerator and denominator of (15) multiply the conjugate complex of the denominator, (15) can be transferred as (16).

$$Z_{invk'}(\omega) = \frac{B(\omega) + jC(\omega)}{A(\omega)} \tag{16}$$

where the detailed expressions of $A(\omega)$, $B(\omega)$ and $C(\omega)$ are shown in (17).

The derivative of phase angle of $Z_{invk'}(\omega)$ can be expressed as (18).

$$\frac{d\varphi(Z'_{invk}(\omega))}{d\omega} = (\arctan(\frac{C(\omega)}{B(\omega)}))' = \frac{(\frac{C(\omega)}{B(\omega)})'}{1 + (\frac{C(\omega)}{B(\omega)})^2} \tag{18}$$

If the derivative of the phase angle of $Z_{invk'}(\omega)$ is equal to zero at $\omega_{ck}$, which can be easily observed from the phase diagram of the fitted transfer function $f(s)$ in (6), the following

$$Z_{invk'}(\omega)=\frac{(K_{pk}-\frac{L_{fk1}L_{fk2}\omega^2}{R_{vk}})\cos(1.5\omega T_{sk})-j(L_{fk1}L_{fk2}C_{fk}\omega^3-(L_{fk1}+L_{fk2})\omega+(K_{pk}-\frac{L_{fk1}L_{fk2}\omega^2}{R_{vk}})\sin(1.5\omega T_{sk}))}{1-L_{fk1}C_{fk}\omega^2+\frac{L_{fk1}\omega}{R_{vk}}\sin(1.5\omega T_{sk})+j\frac{L_{fk1}\omega}{R_{vk}}\cos(1.5\omega T_{sk})} \tag{15}$$

$$\begin{aligned}
A(\omega)&=(1-L_{fk1}C_{fk}\omega^2+\frac{L_{fk1}\omega}{R_{vk}}\sin(1.5\omega T_{sk}))^2+(\frac{L_{fk1}\omega}{R_{vk}}\cos(1.5\omega T_{sk}))^2\\
B(\omega)&=((\frac{L_{fk1}^2}{R_{vk}}-K_{pk}L_{fk1}C_{fk})\omega^2+K_{pk})\cos(1.5\omega T_{sk})\\
C(\omega)&=L_{fk1}^2L_{fk2}C_{fk}^2\omega^5+(\frac{L_{fk1}^2L_{fk2}}{R_{vk}^2}-2L_{fk1}L_{fk2}C_{fk}-L_{fk1}^2C_{fk})\omega^3+(L_{fk1}+L_{fk2}-\frac{K_{pk}L_{fk1}}{R_{vk}})\omega+\ldots\\
&\quad(\frac{-2L_{fk1}^2L_{fk2}C_{fk}\omega^4}{R_{vk}}+(\frac{L_{fk1}^2+2L_{fk1}L_{fk2}}{R_{vk}}+K_{pk}L_{fk1}C_{fk})\omega^2-K_{pk})sin(1.5\omega T_{sk})
\end{aligned} \tag{17}$$

equation will be satisfied based on the calculated $K_{pk}$ and $L_{fk2}$.

$$g(L_{fk1},C_{fk},R_{vk},\omega_{ck})=(\frac{C(\omega)}{B(\omega)})'\Big|_{\omega=\omega_{ck}}=0 \tag{19}$$

Three unknowns ($L_{fk1}$, $C_{fk}$ and $R_{vk}$) exist in two equations (14) and (19). Therefore, the three unknown parameters can be determined using a trial-and-error method.

### *B. Implementation Procedure of the Proposed Gray-Box Parameters Identification and Controller Re-Tuning Method*

Fig. 4 shows the implementation procedure of the proposed gray-box parameters identification and controller re-tuning method. Time-domain simulation of the studied power system is first implemented. If no harmonic instability phenomenon is observed, no further controller re-tuning operation is needed. Otherwise, the terminal impedance frequency responses for all VSCs and grid are measured. Then, the Bode diagrams of the impedance of the left part $Z_S$ and the right part $Z_L$ of PCC are plotted, and potential oscillation frequency is analytically identified from the interaction points. The proposed parameters identification method in this paper is then used to identify the parameters of all of the VSCs. With these identified parameters, the total output impedance of the paralleled VSCs $Z_S$ can be reshaped by reducing $K_{pk}$ or increasing $K_{vk}$, so that the phase angle difference of $Z_S$ and $Z_L$ can be limited within $(-180^0, 180^0)$, which means that the unstable power system is stabilized by re-tuning controller parameters. Finally, the controller parameters re-tuning suggestion can be provided to manufacturer.

## IV. Simulation Verification

In this section, the proposed gray-box parameters identification and controller parameters re-tuning method is validated in both single grid-connected inverter and paralleled inverters system.

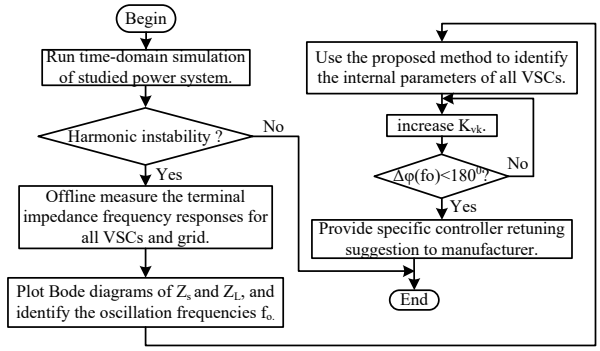


Fig. 4. Flowchart of the proposed gray-box impedance reshaping method for resonance damping.

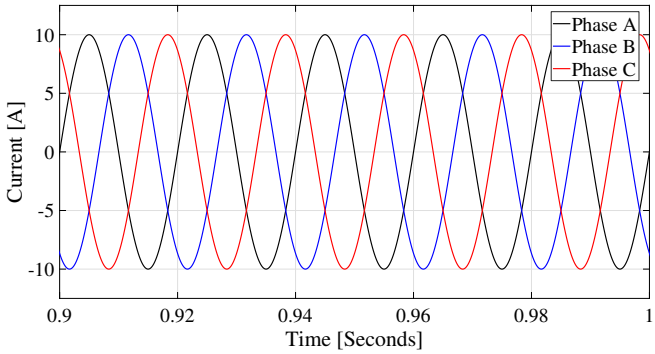


Fig. 5. Time-domain simulation waveforms of three-phase currents when single VSC is connected to the weak grid with $L_g = 3$ mH.

### *A. Case 1: Single VSC*

Fig. 5 shows simulation result of three-phase currents of grid-connected inverter. It can be seen that the grid-connected inverter connected with inductive grid ($L_g = 3$ mH) is stable. However, the system becomes unstable once the grid impedance is increased ($L_g = 8$ mH), as shown in Fig. 6.

System parameters of the exemplified VSC is given in Table

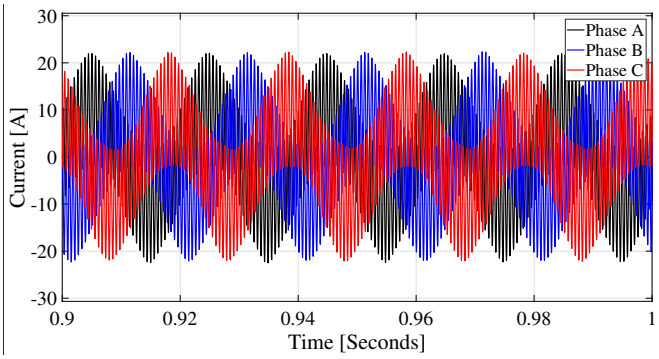


Fig. 6. Time-domain simulation waveforms of three-phase currents when single VSC is connected to the weak grid with $L_g = 8$ mH.

I. The measured terminal impedance frequency response of the VSC is shown as blue solid line in Fig. 7, and frequency response of the fitted 5-order transfer function is shown as red dashed line in Fig. 7. Coefficients of the fitted polynomial transfer function are shown in Table II. According to (11), (14) and (19), parameters of the VSC can be obtained as (20).

$$\begin{aligned} L_{fk2} &= Z = 0.0013 \\ K_{pk} &= \frac{B_0}{A_0} = 20 \end{aligned} \tag{20}$$

By substituting $T_{sk} = 10^{-4}$ s, $\omega_{ck} = -2\pi 1533$ and (20) into (14) and (19), two constraints can be obtained according to $R_{vk} = \frac{L_{fk1}}{K_v C_{fk}}$.

$$\begin{aligned} f_1(L_{fk1}, C_{fk}, K_{vk}) &= 0 \\ f_2(L_{fk1}, C_{fk}, K_{vk}) &= 0 \end{aligned} \tag{21}$$

where the detailed expressions are omitted for simplicity.

The following equation can be obtained from (21).

$$f_3(C_{fk}, K_{vk}) = 0 \tag{22}$$

The solution space has one freedom. One approach is to find the accurate solution in a trial-and-error way. For example, different values of $C_{fk}$ can be first assumed, and the value of $C_{fk}$ which makes the calculated Bode diagram agree with the measured terminal impedance frequency responses is then selected, as shown in Fig. 8.

Fig. 9 shows frequency responses of the calculated terminal impedance formulas with different $C_{fk}$. It can be seen that the calculated frequency response agrees with the original terminal impedance frequency responses when $C_{fk} = 3$ $\mu$F and $K_{vk} = 0.2945$. The identified parameters are given in Table III.

Fig. 10 shows frequency responses of VSC impedance with original controller parameters $Z_{S\_bef}$(blue line) and grid impedance $Z_L$ with $L_g = 8$ mH(black line). It can be seen that phase difference at the interaction point of magnitude curves is $181.36^o$, which indicates that the system is unstable. The analysis results agree with the time-domain simulation result in Fig. 6. One method to stabilize the power system is to increase the capacitor-current-feedback coefficient $K_{vk}$. The

TABLE I
SYSTEM PARAMETERS OF THE EXEMPLIFIED VSC SYSTEM

| Parameter | Value |
|---|---|
| dc-link voltage $V_{dc}$ | 800 V |
| Grid fundamental frequency | 50 Hz |
| Inverter side filter inductance $L_{f1}$ | 3.8 mH |
| Grid side filter inductance $L_{f2}$ | 1.3 mH |
| Filter capacitance $C_f$ | 3 $\mu$F |
| Capacitor-current-feedback coefficient $K_v$ | 0.4 |
| Switching frequency $f_{sw}$ | 10 kHz |
| Sampling frequency $f_{samp}$ | 10 kHz |
| Grid voltage (phase-to-phase) $V_g$ | 380 V |
| Proportional gain of current controller $K_p$ | 20 |
| Integral gain of current controller $K_i$ | 2000 |
| Proportional gain of PLL $K_{ppll}$ | 0.7 |
| Integral gain of PLL $K_{ipll}$ | 3.2 |
| Current reference value $i_d^*$ | 10 A |
| Current reference value $i_q^*$ | 0 |
| Grid inductance $L_g$ | 3 mH |

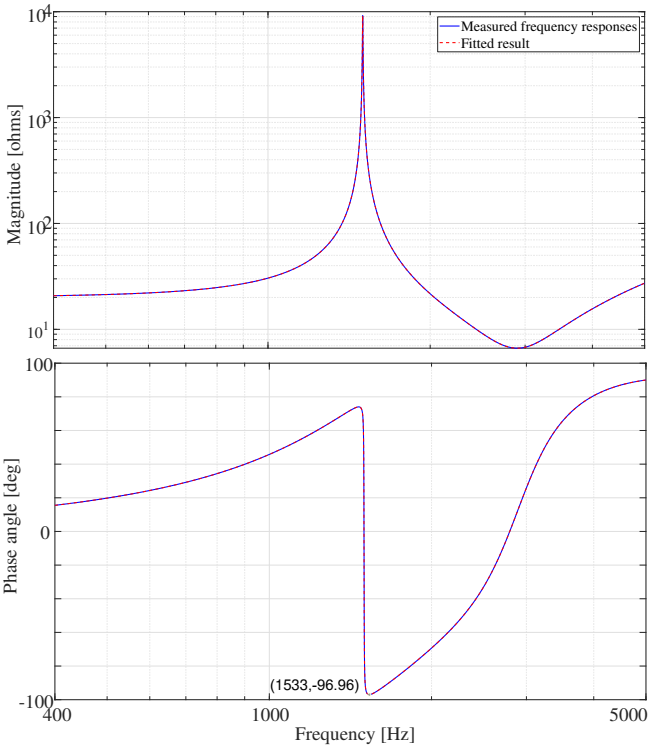


Fig. 7. The measured terminal impedance frequency responses and the fitted result using VF algorithm.

TABLE II
THE COEFFICIENTS OF THE FITTED POLYNOMIAL TRANSFER FUNCTION (6)

| | | | | | |
|---|---|---|---|---|---|
| $A_5$ | $A_4$ | $A_3$ | $A_2$ | $A_1$ | $A_0$ |
| 1 | 1.1955e+05 | 6.2458e+09 | 1.2758e+14 | 5.4790e+17 | 1.0367e+22 |
| $B_5$ | $B_4$ | $B_3$ | $B_2$ | $B_1$ | $B_0$ |
| -10.2279 | 5.7112e+05 | 9.1850e+09 | 2.9526e+15 | 1.8608e+19 | 2.0734e+23 |
| $Z$ | | | | | |
| 0.0013 | | | | | |

Bode diagram of VSC impedance $Z_{S\_aft}$ by increasing $K_{vk}$ from identified value 0.2945 to new value 2.54 is plotted as

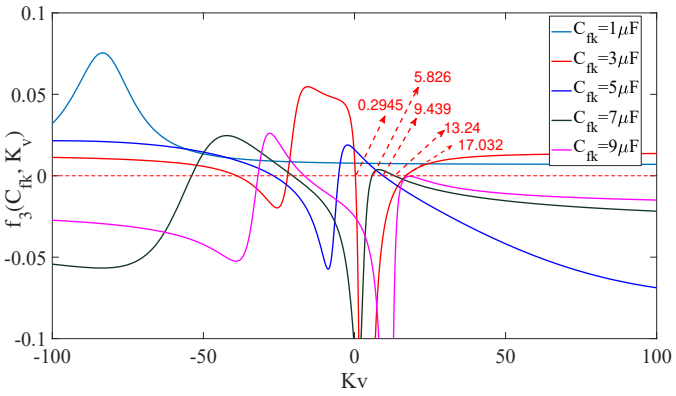


Fig. 8. Waveforms of $f_3(C_{fk}, K_v)$ with different values $C_{fk}$.

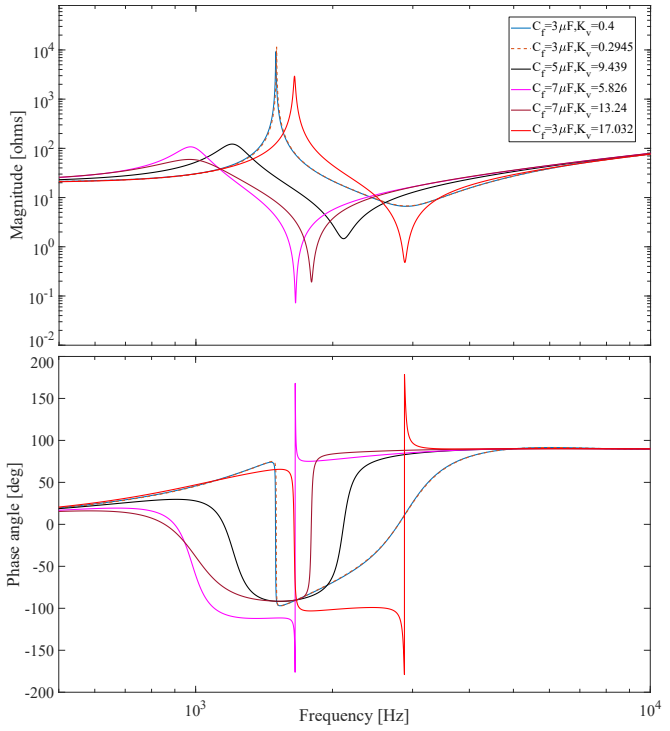


Fig. 9. Bode diagrams of the calculated impedance formulas with assumption of different values of $C_{fk}$.

TABLE III
THE IDENTIFIED PARAMETERS OF THE VSC

| $L_{fk1}$ | $L_{fk2}$ | $C_{fk}$ | $K_p$ | $K_v$ |
|---|---|---|---|---|
| 3.76 mH | 1.3 mH | 3 $\mu$F | 20 | 0.2945 |

the red line in Fig. 10. It can be seen that phase difference at the interaction point of magnitude curves is $178.84^o$, which indicates that the system becomes stable. The simulation result in Fig. 11 shows that the system can be stabilized after $K_{vk}$ is re-tuned.

### *B. Case 2: Three Paralleled VSCs*

Fig. 12 shows simulation results about grid-injected current when three VSCs are connected to grid, where the grid impedance is kept as 3 mH. Comparing with Fig. 5, it can

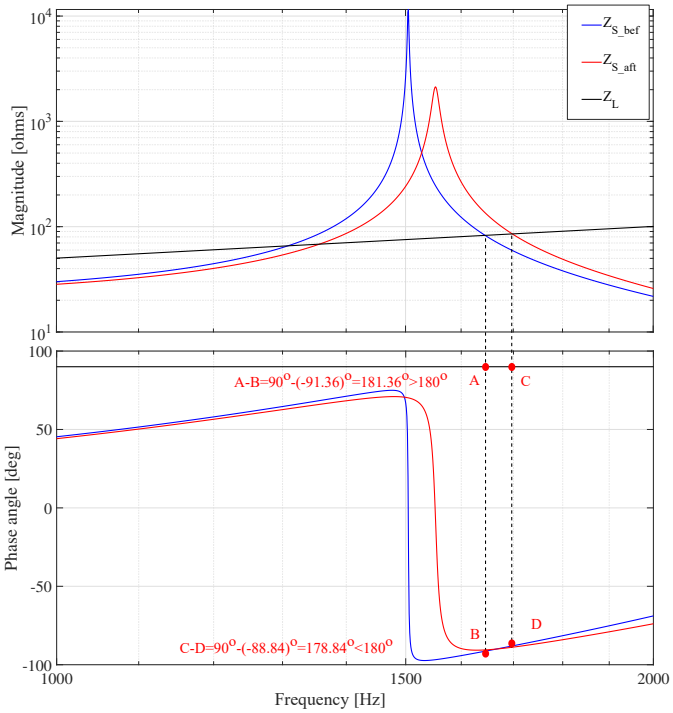


Fig. 10. The Bode diagrams of the terminal impedance formula before and after re-tuning capacitor-current-feedback coefficient $K_{vk}$ for case 1.

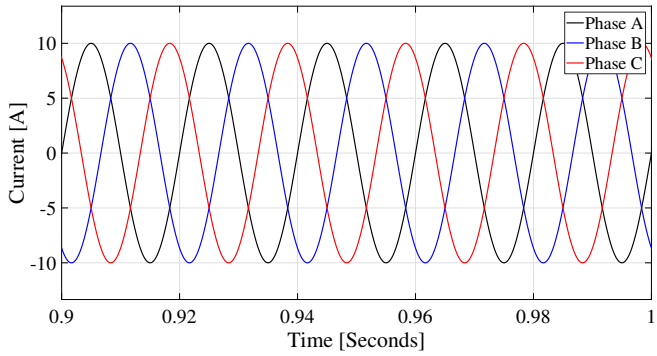


Fig. 11. Time-domain simulation waveforms of three-phase currents when single VSC is connected to the weak grid with $L_g = 8$ mH with capacitor-current-feedback coefficient $K_{vk} = 2.54$.

be seen that the system becomes unstable as the number of VSCs increases.

Fig. 13 shows the terminal impedance frequency responses of three VSCs with original controller parameters $Z_{S\_bef}$ (blue line) and grid impedance $Z_L$ with $L_g = 3$ mH (black line). It can be seen that phase difference at the interaction point of magnitude curves is $182.26^o$, which indicates that the system is unstable. The analysis result agrees with the time-domain simulation result in Fig. 12. The Bode diagram of VSC $Z_{S\_aft}$ impedance by increasing $K_{vk}$ from identified value 0.2945 to new value 2.54 is plotted as the red line in Fig. 13. It can be seen that phase difference at the interaction point of magnitude curves is $179.41^o$, which indicates that the system becomes stable. The simulation result in Fig. 14 shows that the

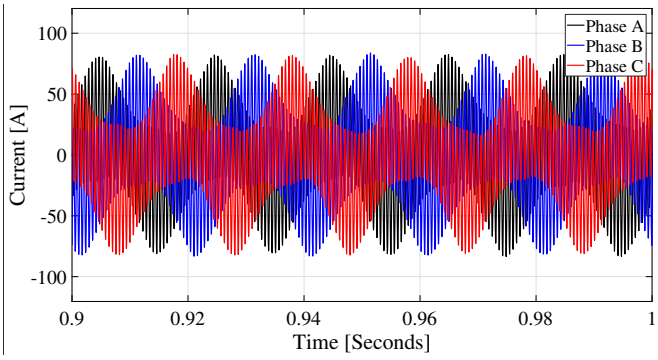


Fig. 12. Simulation results of grid-connected currents when three VSCs are connected to weak grid with $L_g = 3$ mH.

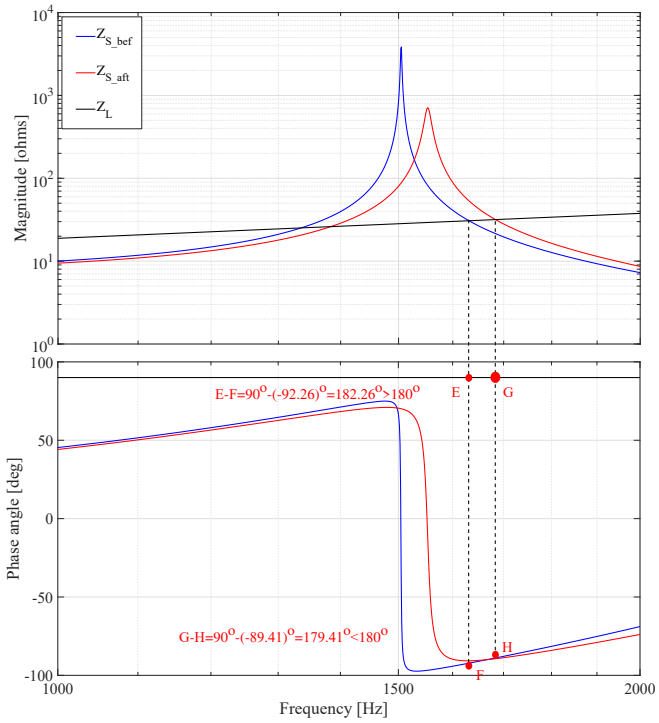


Fig. 13. Bode diagrams of the terminal impedance formula before and after capacitor-current-feedback coefficient $K_{vk}$ re-tuning for case 2.

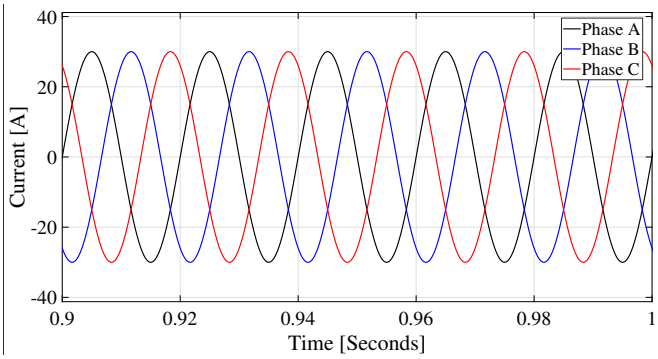


Fig. 14. Simulation results of grid-injected currents when three VSCs are connected to the grid ($L_g = 3$ mH) with capacitor-current-feedback coefficient $K_{vk} = 2.54$.

paralleled VSC system can be stabilized once $K_{vk}$ is re-tuned.

## V. Conclusion

This paper presents a gray-box impedance reshaping method for VSC with LCL filter to enhance system stability. When instability phenomenon occurs, the internal controller parameters of the grid-connected inverter are identified and re-tuned to reshape the terminal impedance characteristics. Simulation results show that the parameters of the LCL filter, proportional coefficient of current controller and the capacitor-current-feedback coefficient are identified from the measured terminal impedance frequency responses by using VF algorithm, and the re-tuned capacitor-current-feedback coefficient can stabilize the system. The proposed gray-box impedance reshaping method is able to provide parameter design and re-tuning guideline for manufacturer even if no internal parameters are known.

## References


[1] P. Bresesti, W. L. Kling, R. L. Hendriks, and R. Vailati, "HVDC connection of offshore wind farms to the transmission system," *IEEE Trans. Energy Convers.*, vol. 22, no. 1, pp. 37–43, Mar. 2007.

[2] N. Flourentzou, V. G. Agelidis, and G. D. Demetriades, "VSC-based HVDC power transmission systems: An overview," *IEEE Trans. Power Electron.*, vol. 24, no. 3, pp. 592–602, Mar. 2009.

[3] R. Pena-Alzola, M. Liserre, F. Blaabjerg, M. Ordonez, and Y. Yang, "LCL-filter design for robust active damping in grid-connected converters." *IEEE Trans. Ind. Informat.*, vol. 10, no. 4, pp. 2192–2203, Nov. 2014.

[4] S. G. Parker, B. P. McGrath, and D. G. Holmes, "Regions of active damping control for LCL filters," *IEEE Trans. Ind. Appl.*, vol. 50, no. 1, pp. 424–432, Jan./Feb. 2014.

[5] W. Zhou, Y. Wang, and Z. Chen, "Decoupled multi-port impedance modelling method of transmission network in inverter-fed power plant," in *Proc. IEEE 2018 International Conference on Smart Grid (icSmartGrid)*, pp. 129–135.

[6] Y. Wang, X. Wang, Z. Chen, and F. Blaabjerg, "Small-signal stability analysis of inverter-fed power systems using component connection method," *IEEE Trans. Smart Grid*, vol. 9, no. 5, pp. 5301–5310, Sep. 2018.

[7] Y. Wang, X. Wang, F. Blaabjerg, and Z. Chen, "Harmonic resonance assessment of multiple paralleled grid-connected inverters system," in *Proc. 2017 IEEE International Power Electronics Conference (ECCE Asia)*, pp. 2070–2075.

[8] R. Pena-Alzola, M. Liserre, F. Blaabjerg, R. Sebastián, J. Dannehl, and F. W. Fuchs, "Analysis of the passive damping losses in LCL-filter-based grid converters," *IEEE Trans. Power Electron.*, vol. 28, no. 6, pp. 2642–2646, Jun. 2013.

[9] S. Zhang, S. Jiang, X. Lu, B. Ge, and F. Z. Peng, "Resonance issues and damping techniques for grid-connected inverters with long transmission cable," *IEEE Trans. Power Electron.*, vol. 29, no. 1, pp. 110–120, Jan. 2014.

[10] W. Yao, Y. Yang, X. Zhang, F. Blaabjerg, and P. C. Loh, "Design and analysis of robust active damping for LCL filters using digital notch filters," *IEEE Trans. Power Electron.*, vol. 32, no. 3, pp. 2360–2375, Mar. 2017.

[11] Y. Guan, Y. Wang, Y. Xie, Y. Liang, A. Lin, and X. Wang, "The dual-current control strategy of grid-connected inverter with LCL filter," *IEEE Trans. Power Electron.*, Early Access.

[12] D. Pan, X. Ruan, C. Bao, W. Li, and X. Wang, "Optimized controller design for LCL-type grid-connected inverter to achieve high robustness against grid-impedance variation," *IEEE Trans. Ind. Electron.*, vol. 62, no. 3, pp. 1537–1547, Mar. 2015.

[13] A. Aapro, T. Messo, T. Roinila, and T. Suntio, "Effect of active damping on output impedance of three-phase grid-connected converter," *IEEE Trans. Ind. Electron.*, vol. 64, no. 9, pp. 7532–7541, Sep. 2017.

[14] X. Wang, F. Blaabjerg, and P. C. Loh, "Passivity-based stability analysis and damping injection for multiparalleled VSCs with LCL filters," *IEEE Trans. Power Electron.*, vol. 32, no. 11, pp. 8922–8935, Nov. 2017.

[15] Y. Song, F. Blaabjerg, X. Wang *et al.*, "Analysis and active damping of multiple high frequency resonances in DFIG system," *IEEE Trans. Energy Convers.*, vol. 32, no. 1, pp. 369–381, Mar. 2017.

[16] H.-C. Chen, P.-T. Cheng, X. Wang, and F. Blaabjerg, "A passivity-based stability analysis of the active damping technique in the offshore wind farm application," *IEEE Trans. Ind. Appl.*, vol. 54, no. 5, pp. 5074 – 5082, Sept.-Oct. 2018.

[17] A. Vidal, A. G. Yepes, F. D. Freijedo, O. Lopez, J. Malvar, F. Baneira, and J. Doval-Gandoy, "A method for identification of the equivalent inductance and resistance in the plant model of current-controlled grid-tied converters," *IEEE Trans. Power Electron.*, vol. 30, no. 12, pp. 7245–7261, Dec. 2015.

[18] A. Vidal, A. G. Yepes, F. D. Freijedo, J. Malvar, O. López, and J. Doval-Gandoy, "A technique to estimate the equivalent loss resistance of grid-tied converters for current control analysis and design," *IEEE Trans. Power Electron.*, vol. 30, no. 3, pp. 1747–1761, Mar. 2015.

[19] S. Mukherjee, V. R. Chowdhury, P. Shamsi, and M. Ferdowsi, "Model reference adaptive control based estimation of equivalent resistance and reactance in grid-connected inverters," *IEEE Trans. Energy Convers.*, vol. 32, no. 4, pp. 1407–1417, Dec. 2017.

[20] J. Koppinen, J. Kukkola, and M. Hinkkanen, "Plug-in identification method for an LCL filter of a grid converter," *IEEE Trans. Ind. Electron.*, vol. 65, no. 8, pp. 6270–6280, Aug. 2018.

[21] M. Amin and M. Molinas, "A gray-box method for stability and controller parameter estimation in HVDC-connected wind farms based on nonparametric impedance," *IEEE Trans. Ind. Electron.*, vol. 66, no. 3, pp. 1872–1882, Mar. 2019.

[22] Z. Liu, H. Wu, W. Jin, B. Xu, Y. Ji, and M. Wu, "Two-step method for identifying photovoltaic grid-connected inverter controller parameters based on the adaptive differential evolution algorithm," *IET Gener. Transm. Distrib.*, vol. 11, no. 17, pp. 4282–4290, Nov. 2017.

[23] W. Zhou, Y. Wang, and Z. Chen, "Reduced-order modelling method of grid-connected inverter with long transmission cable," in *Proc. 2018 IEEE 44th Annual Conference of the IEEE Industrial Electronics Society (IECON)*, pp. 4383–4389.

[24] D. Pan, X. Ruan, C. Bao, W. Li, and X. Wang, "Capacitor-current-feedback active damping with reduced computation delay for improving robustness of LCL-type grid-connected inverter," *IEEE Trans. Power Electron.*, vol. 29, no. 7, pp. 3414–3427, Jul. 2014.

[25] W. Zhou, Y. Wang, and Z. Chen, "A gray-box parameters identification method of voltage source converter using vector fitting algorithm," in *Proc. 2019 IEEE International Power Electronics Conference (ECCE Asia)*, Accepted.

[26] B. Gustavsen and A. Semlyen, "Rational approximation of frequency domain responses by vector fitting," *IEEE Trans. Power Del.*, vol. 14, no. 3, pp. 1052–1061, Jul. 1999.

[27] Y. Wang, X. Wang, F. Blaabjerg, and Z. Chen, "Harmonic instability assessment using state-space modeling and participation analysis in inverter-fed power systems," *IEEE Trans. Ind. Electron.*, vol. 64, no. 1, pp. 806–816, Jan. 2017.